

# CrystEngComm

Accepted Manuscript



This is an *Accepted Manuscript*, which has been through the Royal Society of Chemistry peer review process and has been accepted for publication.

*Accepted Manuscripts* are published online shortly after acceptance, before technical editing, formatting and proof reading. Using this free service, authors can make their results available to the community, in citable form, before we publish the edited article. We will replace this *Accepted Manuscript* with the edited and formatted *Advance Article* as soon as it is available.

You can find more information about *Accepted Manuscripts* in the [Information for Authors](#).

Please note that technical editing may introduce minor changes to the text and/or graphics, which may alter content. The journal's standard [Terms & Conditions](#) and the [Ethical guidelines](#) still apply. In no event shall the Royal Society of Chemistry be held responsible for any errors or omissions in this *Accepted Manuscript* or any consequences arising from the use of any information it contains.

**Mutual transformation between crystalline phases and dielectric properties of coordination polymers with formula of  $[\text{Cd}(\text{N-methylimidazole})_2(\text{H}_2\text{O})_x(\text{glutarate})] \cdot n\text{H}_2\text{O}$  ( $x = 0$  or  $1$ ;  $n = 0$  or  $4$ )**

Chen Xue,<sup>a,b</sup> Heng Xu,<sup>\*b</sup> Rong-Yi Huang,<sup>b</sup> Xiao-Ming Ren<sup>\*ac</sup>

<sup>a</sup> State Key Laboratory of Materials-Oriented Chemical Engineering and College of Science, Nanjing University of Technology, Nanjing 210009

<sup>b</sup> Anhui Key Laboratory of Functional Coordination Compounds, School of Chemistry and Chemical Engineering, Anqing Normal University, Anqing 246003, P. R. China

<sup>c</sup> College of Materials Science and Engineering, Nanjing University of Technology, Nanjing 210009

Tel.: +86 25 58139476

Fax: +86 25 58139481

Email: [xmren@njtech.edu.cn](mailto:xmren@njtech.edu.cn)

**Abstract**

We successfully achieved the crystals of two pseudo-polymorphs, Cd(NMIZ)<sub>2</sub>(glutarate) (**1**) and [Cd(NMIZ)<sub>2</sub>(H<sub>2</sub>O)(glutarate)]·4H<sub>2</sub>O (**2**) where NMIZ represents N-methylimidazole, through controlling the crystalline temperature. The Cd<sup>2+</sup> ion forms distorted trigonal prism coordination geometry with two nitrogen atoms from two NMIZ ligands and four oxygen atoms from two carboxylates in **1**, while pentagonal bipyramid coordination geometry with two nitrogen atoms from two NMIZ ligands, four oxygen atoms from two carboxylates and one oxygen atom from coordinated water in **2**. The glutarates acted as μ<sub>2</sub>-bridging ligands connect the coordination polyhedral to form coordination polymeric chain in both **1** and **2**. The coordination polymeric chains are arranged in parallel arrays and held together via intermolecular van der Waals force into three-dimensional structure in **1**, whereas two-dimensional bi-layers, where the lattice water molecules locate between bi-layers and are anchored to the coordination polymeric chain via intermolecular H-bonds in **2**. The crystalline phase transformation is reversible between **1** and **2** as well as between **2** and **3**. Three different crystalline phases show distinct dielectric features. The dielectric permittivity is related to the amount of water in lattice with the order **2** > **3** > **1**, this is due to that the orientation of polar water molecules in crystal is able to obey the change of external electric field and transfer the polarization.

Keywords: Coordination polymer, pseudo-polymorph, crystalline phase transformation, dielectric property

## Introduction

Polymorphism or pseudo-polymorph is one of the most fascinating phenomena in solid state chemistry and indeed is a “difficult” phenomenon. In spite of the huge efforts of many researchers our knowledge of the phenomenon is still embryonic, the relationship between growth of a crystalline phase and nucleation of the first crystallites is often mysterious<sup>1</sup> and remains poorly understood, therefore it is difficult to control and predict the emergence of different forms at present stage.<sup>2-6</sup>

Generally, the different crystal forms may display a range of distinct physico-chemical properties due to their diverse crystal arrangements.<sup>7-11</sup> The well known example is diamond and graphite, which are two allotropes of carbon. The carbon atoms are bonded together in a tetrahedral lattice arrangement in diamond, whereas in sheets of a hexagonal lattice in graphite. Diamond is the hardest known natural substance, while graphite is very soft matter. Another interesting case concerns two polymorphs of conductive metal-organic framework Tl(TCNQ) where TCNQ = 7, 7, 8, 8-tetracyanoquinodimethane. The structure difference between two polymorphs of Tl(TCNQ) involves the arrangement of adjacent TCNQ stacks. One polymorph shows the 90° arrangement of adjacent TCNQ stacks occurred in the structures of the Na<sup>+</sup>, K<sup>+</sup>, and Rb<sup>+</sup> TCNQ analogues and weak semi-conductivity ( $\sigma = 2.4 \times 10^{-4} \text{ S}\cdot\text{cm}^{-1}$  at room temperature), whereas another polymorph exhibits the parallel arrangement of the TCNQ stacks observed in the Cs(TCNQ) network and much higher conductivity ( $\sigma = 5.4 \times 10^{-1} \text{ S}\cdot\text{cm}^{-1}$  at room temperature).<sup>12</sup>

Polymorphism or pseudo-polymorph of organic substances is a well-known phenomenon, however, it is scarce in the field of coordination compounds, particularly coordination polymers,<sup>13</sup> which are constructed from metal ions/metal ion clusters and bridging organic ligands. In the context of coordination polymer polymorphism, it is notable that, by comparison of open-shell transition metal coordination polymers,<sup>14, 15</sup> the relative rich structural polymorphisms occur in the coordination polymers built from the main group metal ions,<sup>12, 16-18</sup> transition metal

ions with  $d^n$  electronic configuration ( $n = 0$  or  $10$ ) and rare earth metal ions.<sup>19-26</sup> This situation is probably related to the fact that the coordinate bonds between the metal ion with closed-shell electronic configuration (or the rare earth metal ion where f-electrons constitute inner shells) and coordinate atoms show non-directional character of ionic bonds and have equal influence in all directions; the coordinate sphere of such a metal ion adopts easily in different geometries, which result in the distinct molecule arrangement in crystal, but the exact mechanism is still unclear.

It is important to obtain a particular polymorph under reproducible conditions, although this is not always easy to achieve. Thus, the isolation, identification and characterization of different polymorphs of coordination polymer are very useful for better understanding the factors that control the nucleation of polymorphic materials and the growth of the desired polymorph with fascinating physical property.

In this paper, we report three different crystalline phases with formula of  $[\text{Cd}(\text{N-methylimidazole})_2(\text{H}_2\text{O})_x(\text{glutarate})] \cdot n\text{H}_2\text{O}$  ( $x = 0$  or  $1$ ;  $n = 0$  or  $4$ ). The pure phases of  $\text{Cd}(\text{N-methylimidazole})_2(\text{glutarate})$  and  $[\text{Cd}(\text{N-methylimidazole})_2(\text{H}_2\text{O})-(\text{glutarate})] \cdot 4\text{H}_2\text{O}$  were isolated by controlling crystallization temperature. The structural transformation between the different crystalline phases and the dielectric property is investigated for three crystalline phases.

## Experimental

### Chemicals and materials

The chemicals, N-methylimidazole (abbr. as NMIZ), glutaric acid and  $\text{Cd}(\text{OAc})_2 \cdot 2\text{H}_2\text{O}$ , as well as solvents employed were of reagent grade and used without further purification.

### Preparations of compounds

**$\text{Cd}(\text{NMIZ})_2(\text{glutarate})$  (1) and  $[\text{Cd}(\text{NMIZ})_2(\text{H}_2\text{O})(\text{glutarate})] \cdot 4\text{H}_2\text{O}$  (2).**  $\text{Cd}(\text{OAc})_2 \cdot 2\text{H}_2\text{O}$  (1.336 g, 5 mmol) and glutaric acid (0.663 g, 5 mmol) were dissolved in 35 mL methanol and heated with intensely stirring at 60 °C to evaporate

methanol to dryness. To the dried mixture, the ethanol–deionized water solution (20 mL with V/V = 1:1) of N-methylimidazole (0.842 g, 10 mmol) was added, and then the mixture was stirred at 80 °C for 2 hours to give clear solution. Such solution was divided into two parts (A and B).

The solution in part A was evaporated at 63 °C in an airflow drying oven over two days. Colorless block-shaped crystals with a formula of Cd(NMIZ)<sub>2</sub>(glutarate) were isolated and washed with ethanol. Yield: ~71% (based on Cd(OAc)<sub>2</sub>·2H<sub>2</sub>O). Elemental microanalysis calculated for C<sub>13</sub>H<sub>18</sub>N<sub>4</sub>O<sub>4</sub>Cd (**1**): C, 38.39; H, 4.46; N 13.78%. Found: C, 37.82; H, 4.41; N, 13.11%. IR spectrum (KBr pellet, cm<sup>-1</sup>) and the assignments for the listed bands: 3120s, 3098s (ν<sub>C-H</sub> of imidazole ring); 2964m, 2944ms (ν<sub>C-H</sub> of –CH<sub>3</sub>); 1552s (ν<sub>as(C=O)</sub> of COO<sup>-</sup>) 1407 (ν<sub>s(C=O)</sub> of COO<sup>-</sup>); 1105s (δ<sub>C-C-C</sub> of alkyl chain), where ‘s’, ‘ms’ and ‘m’ represent the band intensity being strong, medium strong and medium, respectively.

The solution in part B was evaporated at ambient temperature for 7–9 days to give colorless rod-shaped crystals with formula of [Cd(NMIZ)<sub>2</sub>(H<sub>2</sub>O)(glutarate)]·4H<sub>2</sub>O (**2**). Yield: ca. 78% (based on Cd(OAc)<sub>2</sub>·2H<sub>2</sub>O). Elemental microanalysis calculated for C<sub>13</sub>H<sub>28</sub>N<sub>4</sub>O<sub>9</sub>Cd (**2**): C, 31.43; H, 5.68; N 11.28%. Found: C, 32.09; H, 5.30; N, 11.76%. IR spectrum (KBr pellet, cm<sup>-1</sup>) and the assignments for the listed bands: 3409 (ν<sub>O-H</sub> of H<sub>2</sub>O); 3103ms (ν<sub>C-H</sub> of imidazole ring); 2950 (ν<sub>C-H</sub> of –CH<sub>3</sub>); 1566s (ν<sub>as(C=O)</sub> of COO<sup>-</sup>); 1407(ν<sub>s(C=O)</sub> of COO<sup>-</sup>); 1101 (δ<sub>C-C-C</sub> of alkyl chain).

**[Cd(NMIZ)<sub>2</sub>(H<sub>2</sub>O)(glutarate)] (**3**)**. Crystals of **2** were heated at 50 °C for 6 hours to give **3**. Elemental microanalysis calculated for C<sub>13</sub>H<sub>20</sub>N<sub>4</sub>CdO<sub>5</sub> (**3**): C, 36.76; H, 4.75; N 13.19%. Found: C, 36.51; H, 4.67; N, 13.69%. IR spectrum (KBr pellet, cm<sup>-1</sup>) and the assignments for the listed bands: 3394 (ν<sub>O-H</sub> of H<sub>2</sub>O); 3106 (ν<sub>C-H</sub> of imidazole ring); 2960 (ν<sub>C-H</sub> of –CH<sub>3</sub>); 1575 (ν<sub>as(C=O)</sub> of COO<sup>-</sup>); 1409 (ν<sub>s(C=O)</sub> of COO<sup>-</sup>); 1108 (δ<sub>C-C-C</sub> of alkyl chain).

It is worth mentioning that there is slight difference between the found and calculated values of C, H and N elemental analyses for **1** and **2**, this is due to the sample of **1** absorbed a little amount water and the sample of **2** lost a little amount lattice water before elemental analysis. The elemental microanalysis for C, H and N is

in well agreement with the calculation based on the formula  $C_{13}H_{18}N_4O_4Cd \cdot 0.5H_2O$  (C, 37.56; H, 4.41; N 13.48%) for **1** and  $C_{13}H_{18}N_4O_4Cd \cdot 4.5H_2O$  (C, 32.01; H, 5.58; N 11.49%) for **2**.

### Physical measurements

Elemental analyses for C, H and N were performed with an Elementar Vario EL III analytic instrument. FT-IR spectra were carried on an IF66V FT-IR spectrophotometer using KBr pellets within a range of 4000-400  $cm^{-1}$ . Raman spectra were recorded using a Renishaw Raman Microscope spectrometer. An  $Ar^+$  laser emitting at 532 nm was used in which its output power was limited to 5% in order to avoid sample decomposition. Powder X-ray diffraction (PXRD) data were collected on a Bruker D8 diffractometer, operated at 40 kV and 40 mA, with Cu  $K\alpha$  radiation ( $\lambda = 1.5418 \text{ \AA}$ ), and the measurement was performed at ambient temperature in the range  $2\theta = 5-55^\circ$  with  $0.01^\circ/\text{step}$ .

Thermogravimetric analysis (TGA) were performed with a TA2000/2960 thermogravimetric analyzer in the temperature range 20–800  $^\circ C$  under nitrogen atmosphere; the polycrystalline sample was placed in  $Al_2O_3$  crucible, the heating rate is  $10^\circ C \cdot \text{min}^{-1}$  and the nitrogen flow rate is  $50 \text{ mL} \cdot \text{min}^{-1}$ .

Temperature- and frequency-dependent dielectric permittivity ( $\epsilon'$ ) and dielectric loss ( $\epsilon''$ ) were measured for polycrystalline sample using a Concept 80 system. The ac electric field frequencies span from  $10^2$  to  $10^7$  Hz. The pressed pellet was sandwiched by copper electrodes during the measurement. The pellet was made under a static pressure of 10 MPa, with 1.11 mm thickness and  $78.5 \text{ mm}^2$  area (mass = 0.243 g) for **1**, 2.3 mm thickness and  $78.5 \text{ mm}^2$  area (mass = 0.361g) for **2**.

### X-ray Crystallography

X-ray single crystal structural data of **1** and **2** were collected at 293 K graphite monochromated Mo- $K\alpha$  radiation ( $\lambda = 0.71073 \text{ \AA}$ ) on a Bruker-SMART CCD area detector. Data reductions and absorption corrections were performed with the SAINT and SADABS software packages,<sup>27</sup> respectively. The structures were solved by a

direct method using the SHELXL-97 software package.<sup>28</sup> The structure refinement was done with SHELXL-97 for **1** while with SHELXL-2013 for **2**. The non-hydrogen atoms were anisotropically refined using the full-matrix least-squares method on  $F^2$ . All hydrogen atoms besides those in water molecules were geometrically fixed and placed in ideal positions. The hydrogen atoms in water molecules were found from the difference map of electron density and their coordinates were refined while the O-H bond lengths were constrained.  $U_{\text{iso}}$  of all hydrogen atoms are not refined and constrained to be  $1.2U_{\text{iso}}$  or  $1.5U_{\text{iso}}$  of the attached atoms. The details about data collection, structural refinement and crystallography are listed in Table 1. The selected bond lengths and bond angles are summarized in Table 2 for **1** and **2**.

## Results and discussion

### Crystal structures of **1** and **2**

Coordination polymer **1** crystallizes in monoclinic space group  $P2_1/c$  (no. 14); its asymmetric unit is comprised of one  $\text{Cd}^{2+}$  ion, two NMIZ molecules and one glutarate. As shown in Figure 1a,  $\text{Cd}^{2+}$  ion is coordinated by four oxygen atoms from two different glutarates, two nitrogen atoms from two individual NMIZ molecules to form the distorted trigonal prism coordination geometry, where three oxygen atoms, two oxygen atoms from the same carboxylate and one oxygen atom from another carboxylate, construct one bottom surface of the distorted trigonal prism; two nitrogen atoms and one oxygen atom from carboxylate build another bottom surface of the distorted trigonal prism (ref. Figure 1b). Two carboxylate planes (made by three atoms of COO) are almost perpendicular to each other with a dihedral angle of  $86.6^\circ$ .

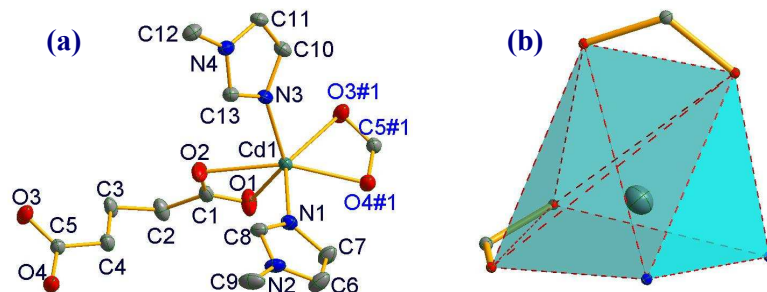


Figure 1: (a) Molecular structure of **1** where H atoms were omitted for clarity, non-hydrogen atoms labeled with 20% probability thermal ellipsoids and symmetry code #1 =  $-1+x, y, z$  and (b) mono-capped square pyramid coordination geometry of  $\text{Cd}^{2+}$  ion in **1**.

The bond lengths and angles in the coordination trigonal prism of **1**, summarized in Table 2, are within the expected values ranges and comparable to those in the polymorph recently reported by Yeşil and coworkers.<sup>29</sup> The glutarate acts as a  $\mu_2$ -bridging ligand to connect two  $\text{Cd}^{2+}$  ions into coordination polymeric chain along  $a$ -axis direction (ref. Figure 2a and 2b), the adjacent coordination polymeric chains show the same orientation along  $c$ -axis (Figure 2a), while antiparallel and interdigitated fashion along  $b$ -axis (Figure 2b). The coordination polymeric chains extend into three-dimensional structure via intermolecular van der Waals forces.

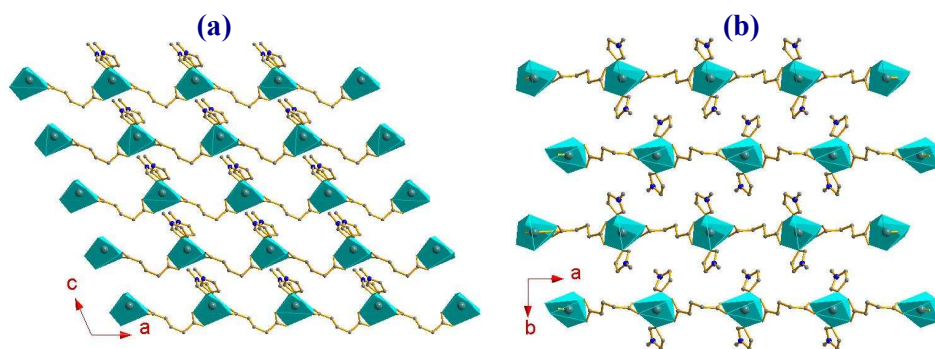


Figure 2: Packing structures of **1** viewed along (a)  $b$ -axis and (b)  $c$ -axis directions.

The coordination sphere of  $\text{Cd}^{2+}$ , the conformation of the glutarate ligand and the packing structure in **1** are analogous to its polymorph,<sup>29</sup> while the distinction between the structures of **1** and the polymorph reported concern (1) the  $\text{Cd}^{2+}$  ion coincides with a mirror plane in the reported polymorph of **1** which leads to its asymmetric unit being equal to one half of that in **1**. (2) The glutarate ligand in **1** is ordering whereas disordering in the reported polymorph of **1**.

Crystal of **2** belongs to orthorhombic system, space group  $Pcca$  with one half  $\text{Cd}^{2+}$  ion, one half glutarate, one NMIZ, two and half  $\text{H}_2\text{O}$  molecules in an asymmetric unit (ref. Figure 3a). Cd1, O1W and C3 atoms occupy the Wyckoff position 4c with site symmetry  $C_2$  (twofold rotation axis) and other atoms reside in the Wyckoff position 8f

with site symmetry  $C_1$ .  $\text{Cd}^{2+}$  ion adopts heptacoordination with pentagonal bipyramid coordination geometry, and the coordination sphere is consisted of five oxygen atoms (from one  $\text{H}_2\text{O}$  and two equivalent carboxylates) and two nitrogen atoms (from two equivalent NMIZ molecules). Five oxygen atoms construct the equatorial plane, and two nitrogen atoms occupy at the apexes of the pentagonal bipyramid (ref. Figure 3b). The coordination pentagonal bipyramid has  $C_2$  point group symmetry; its twofold rotation axis passes through O1W and Cd1 and is parallel to  $b$ -axis. It is distinct from **1** that two carboxylate planes (COO) are almost parallel to each other with a dihedral angle of  $4.2^\circ$  in the coordination pentagonal bipyramid of **2**. As displayed in Table 2, the Cd-O bond distances span from 2.228(3) to 2.4766(17) Å and the Cd-N bond length is 2.287(2) Å; the  $\angle\text{O-Cd-O}$  angles fall within a ranges of  $52.69(5)$ – $168.43(7)^\circ$ , the  $\angle\text{O-Cd-N}$  angles span from  $83.16(7)$  to  $98.08(7)^\circ$  and  $\angle\text{N-Cd-N} = 167.79(10)^\circ$  in the coordination pentagonal bipyramid.

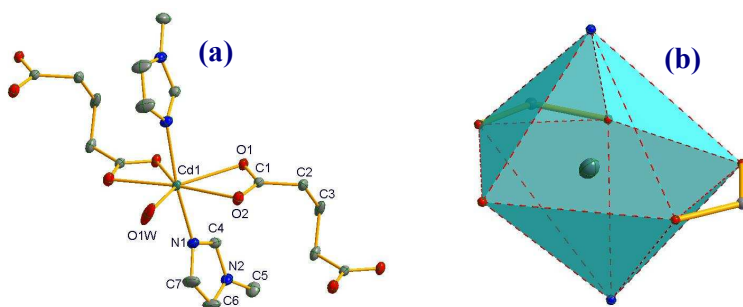
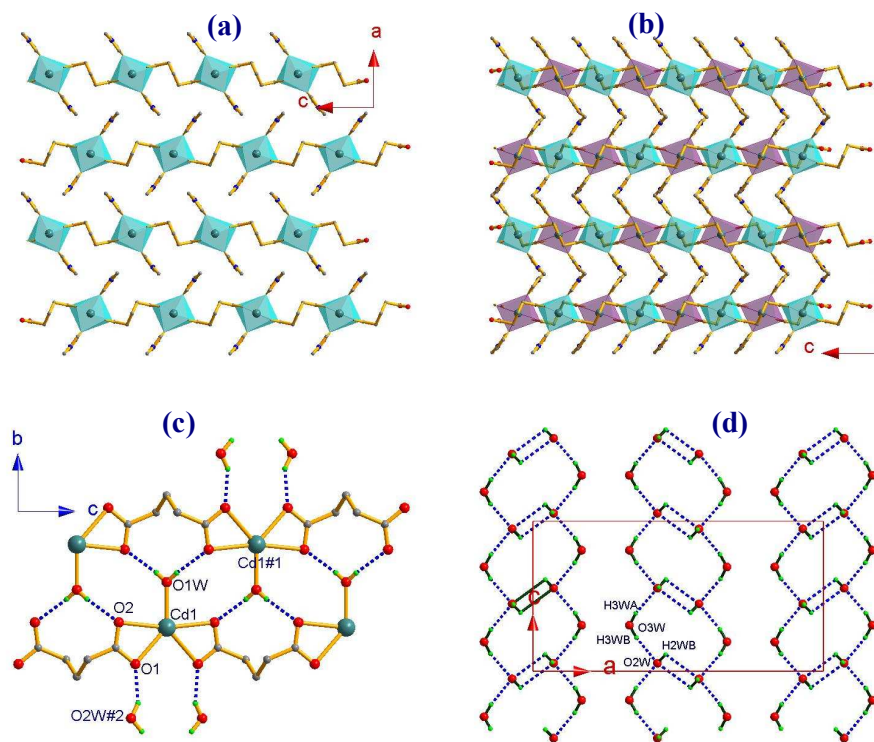


Figure 3: (a) Molecular structure of **2** where H atoms were omitted for clarity, non-hydrogen atoms labeled with 20% probability thermal ellipsoids (b) pentagonal bipyramid coordination geometry of  $\text{Cd}^{2+}$  ion in **2**.

It is similar to **1** that the glutarate acts also as a  $\mu_2$ -bridging ligand in **2** to connect two coordination pentagonal bipyramids into coordination polymeric chain along  $c$ -axis direction (ref. Figure 4a), the adjacent coordination polymeric chains, along  $a$ -axis direction, are related by a glide plane (which is perpendicular to  $c$ -axis and translates along  $a$ -axis by 1/2 unit) together with a translation along  $c$ -axis by 1/2 unit. The coordination polymeric chains are held together through intermolecular van der Waals forces to arrange into a single molecule layer, which is perpendicular to  $b$ -axis. Two neighboring single molecule layers are related to each other via a translation

along *c*-axis by 1/2 unit and connected into a bilayer via intermolecular H-bonds between the coordinated H<sub>2</sub>O molecules and O atoms of carboxylates in the neighboring single molecule layer, with hydrogen bond parameters  $d_{O1W...O2\#2} = 2.715(2)$  Å and  $\angle O1W-H1WA...O2\#2 = 171^\circ$  where the symmetric code #2 = 1-x, 2-y, 2-z (see Figure 4b and 4c). The lattice H<sub>2</sub>O molecules form H-bonding double chain along *c*-axis with hydrogen bond geometric parameters of  $d_{O2W...O3W} = 2.799(3)$  Å and  $\angle O3W-H3WA...O2W = 172^\circ$ ,  $d_{O2W\#3...O3W} = 2.795(3)$  Å and  $\angle O3W-H3WB...O2W\#3 = 160^\circ$ ,  $d_{O2W\#4...O2W} = 2.870(3)$  Å and  $\angle O2W-H2WB...O2W\#4 = 118^\circ$  where the symmetric code #3 = x, 1-y, 0.5+z and #4 = 1-x, 1-y, -z; the H-bonding supramolecular chains are aligned into H<sub>2</sub>O molecule layer (ref. Figure 4b). The H<sub>2</sub>O molecule double chains are anchored to the coordination polymeric chains via intermolecular H-bonds formed between O1 and O2W with bond parameters of  $d_{O2W...O1\#5} = 2.733(2)$  Å and  $\angle O2W-H2WA...O1\#5 = 179^\circ$  where the symmetric code #5 = x, y, -1+z (ref. Figure 4c). The H<sub>2</sub>O molecule layer and coordination polymeric bilayer alternate to form a three-dimensional supramolecular structure along *b*-axis, which is shown in Figure 4e.



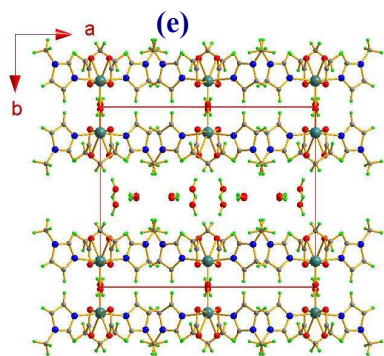


Figure 4: (a, b) Mono- and bi-layers of coordination polymers (c) H-bonds within a coordination polymeric double layer and between the coordination polymeric double layer and the lattice H<sub>2</sub>O layers (d) H-bonds in lattice H<sub>2</sub>O layer (e) alternative coordination polymeric double layer and lattice H<sub>2</sub>O layer viewed along c-axis for **2**.

### TG analyses of 1-3

TG curves of **1–3** are displayed in Figure 5a, which showed three steps of successive mass losses for **1** while four distinct mass losses for **2** and **3**, respectively, in the temperature ranges 20–800 °C. As shown in Figure 5b, DSC curve of **1** presented an endothermic peak at 214 °C associated with one half equivalents N-methylimidazole per formula unit ( $[\text{Cd}(\text{NMIZ})_2(\text{glutarate})]$ ) removed, and the 9.81% of mass loss between 160 and 220 °C is close to the theoretical value (10.1%). The second endothermic peak appeared at 298 °C in DSC plot, accompanied by a mass loss of 30.1% between 220 and 311 °C in its TG plot, which is attributed to the remained N-methylimidazole being wholly removed with the theoretical mass loss percentage of 30.3%. The third endothermic peak occurred at 450 °C in DSC plot, with a mass loss of 27.5% between 311 and 541 °C in TG plot, this losing mass process is due to the decomposition of the glutarate with a theoretical mass loss of 28.0%. The percentage of residual is 31.6%, meaning that the final product is CdO.

As shown in Figure 5a, the process of losing water molecules started at room temperature and ended around 100 °C with a mass loss of 10.3% (between room temperature and 104 °C) for **2**, while the theoretical percentage lost both lattice and coordinated water molecules, according to the formula

$[\text{Cd}(\text{NMIZ})_2(\text{H}_2\text{O})(\text{glutarate})]\cdot 4\text{H}_2\text{O}$ , is 18.1%, this discrepancy between the observed and theoretical mass loss is due to the fact that the part of water molecules had lost before the TG measurement and the lost water molecules were estimated to be two equivalents per formula  $[\text{Cd}(\text{NMIZ})_2(\text{H}_2\text{O})(\text{glutarate})]\cdot 4\text{H}_2\text{O}$ . No sizable mass loss was observed below 72 °C in the TG plot of **3**. The first step of mass loss between 72 and 100 °C is ascribed to the coordinated water removed, the mass loss percentage (3.0%) observed is less than the theoretical value 4.2% calculated from the formula  $\text{Cd}(\text{NMIZ})_2(\text{H}_2\text{O})(\text{glutarate})$  owing to some water molecules released before TG measurement. Such low temperature to release the coordinated water molecules demonstrates that the coordinated  $\text{H}_2\text{O}$  is loosely bound to  $\text{Cd}^{2+}$  ion. It was noted that above 100 °C, the water-free samples of **2** and **3** experienced the same losing mass processes in the related temperature intervals as **1**, namely, lost one half equivalents N-methylimidazole per formula unit followed by releasing whole N-methylimidazole ligands and, finally, decomposition of glutarate ligands to give the product  $\text{CdO}$ . This means that **2** and **3** are probably transformed into **1** after water molecules were completely removed, this presumption was further confirmed by Raman spectra and PXRD measurements.

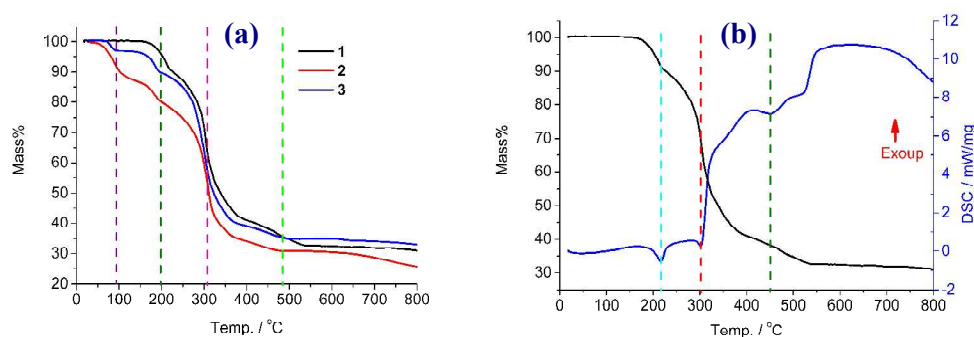


Figure 5: (a) TG plots of **1–3** in the temperature ranges 20–800 °C (b) TG-DSC of **1**.

### Structural transformations between different crystalline phases

On the basis of TG analysis, we found that the lattice water molecules were removable at room temperature; however, the coordinated water starts to release around 72 °C in **2**. Thus, the samples of **2** were heated under 50 °C (the product

corresponds to **3**) and 100 °C (the products corresponds to **1**), respectively, in order to stepwisely remove the lattice water molecules and the coordinated water. Figure 6a shows the PXRD patterns in  $2\theta = 5\text{--}30^\circ$  regions, where the plots I and V represent correspondingly the simulated profiles of **2** and **1**, and the plots II–IV correspond sequentially to the experimental profiles of the as-synthesized sample of **2**, the annealed samples under 50 °C (compound **3**) and 100 °C (compound **1**) of **2**. The samples of **2** annealed under 50 °C (compound **3**) and 100 °C (compound **1**) displayed the analogous PXRD pattern to **1**, indicating that **2** was transformed into **1** as water molecules was wholly lost. The structural transformation between **1** and **2** is reversible, as illustrated in Figure 6b, the original structure of **2** can be restored when the water-free sample of **2** was exposed to excessive moisture at ambient temperature.

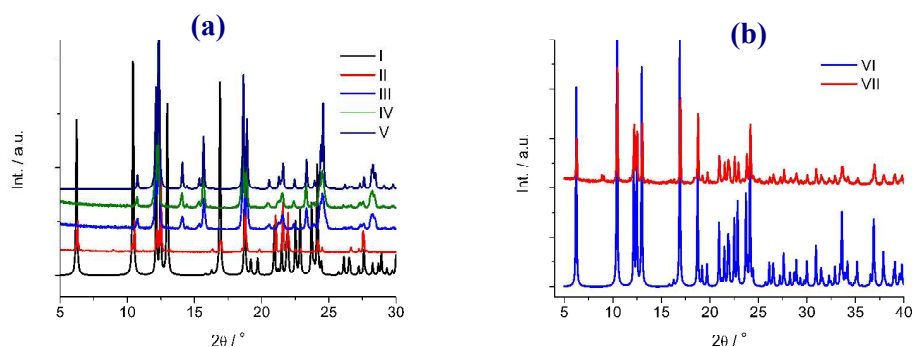


Figure 6 (a) PXRD patterns where I and V represent the simulated profiles of **2** and **1**, II–IV correspond sequentially to the experimental profiles of the as-synthesized sample, the annealed ones under 50 °C (compound **3**) and 100 °C (compound **1**) of **2**, respectively. (b) PXRD patterns: plot VII stands for the simulated profile of **2** and plot VI represents the experimental profile of water-free sample of **2** exposed to excessive moisture.

Raman spectra of **1** and the samples of **2** annealed under 50 °C (compound **3**) and 100 °C (compound **1**) are shown in Figure 7, indicating that the spectra between **1** and the sample of **2** annealed under 50 °C (compound **3**) are distinct, whereas the spectra between **1** and the sample of **2** annealed under 100 °C (compound **1**) are almost the same. This observation further confirmed that **2** was transformed into **1** when the lattice and coordinated water molecules were entirely removed.

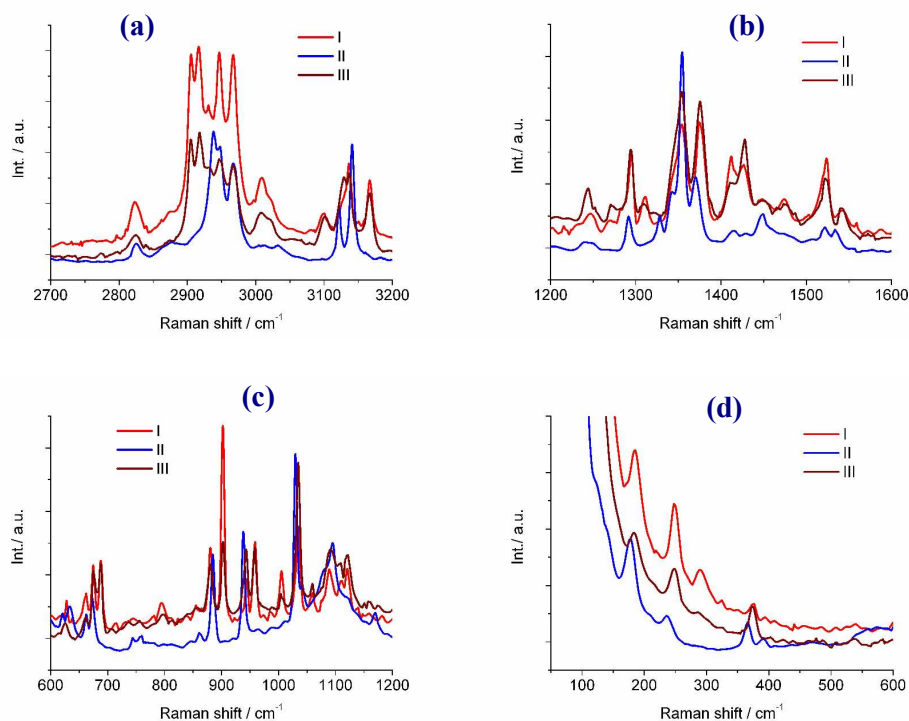


Figure 7 (a-d) Raman spectra of **1** (I), the samples of **2** annealed under 50 °C (II) 100 °C (III) in the selected wavenumber ranges.

### Dielectric properties of 1-3

The complex permittivity formalism has been employed to reveal significant information about the chemical and physical behavior of the electrical and dielectric properties, it is expressed as:

$$\varepsilon^*(\omega) = \varepsilon'(\omega) + j\varepsilon''(\omega) \quad (1)$$

Where  $\varepsilon'(\omega)$  and  $\varepsilon''(\omega)$  are the real and imaginary parts of the dielectric constant, respectively. The variation of  $\varepsilon'(\omega)$  and  $\varepsilon''(\omega)$  with temperature at selected frequencies are illustrated in Figure 8a and 8b for **1**, respectively. The frequency dependent  $\varepsilon'(\omega)$  and  $\varepsilon''(\omega)$  are correspondingly displayed in Figure 8c and 8d for **1**. The measurements were performed in a heating/cooling cycle, and the temperatures span from -150 to 145 °C. The dielectric permittivity,  $\varepsilon'(\omega)$ , is almost constant (ca. 5.4) in the plot of  $\varepsilon'(\omega)$  vs. T below 20 °C and the  $\varepsilon''(\omega)$  value is less than 1.0 in the plot of  $\varepsilon''(\omega)$  vs. T below 70 °C. As temperature increases, the real and imaginary parts of complex permittivity increase quickly and the dispersion is very strong in high

temperature at low frequencies. Such a thermally assisted dielectric dispersion is due to that the orientation of molecules in crystal **1** is able to obey the change of external electric field more easily in higher temperature.<sup>30</sup> As shown in Figure 8c and 8d, the dielectric permittivity in the  $\epsilon'(\omega)$ - $f$  plot of **1** is maintained at 5–7 over the frequency range of  $10^2$ – $10^7$  Hz below 50 °C, and then increases with rising temperature. The  $\epsilon'(\omega)$  value rises rapidly when the temperature is above 100 °C under a frequency of 100 Hz. The dielectric permittivity  $\epsilon'(\omega)$  drops with increasing frequency in the region of  $10^2$ – $10^5$  Hz (see Figure 8c), demonstrating that the dynamic dipole motion cannot follow the switching of the applied ac electric field under higher frequencies (when  $f > 10^5$  Hz). Corresponding to the dielectric permittivity  $\epsilon'(\omega)$  drop, no clear broad peak appears in the  $\epsilon''(\omega)$ - $f$  plot in the  $10^2$ – $10^5$  Hz region (see Figure 8d), but this probably occurs in the frequency region below  $10^2$  Hz.

The dielectric measurements were carried out for three successive heating/cooling cycles between -150 and 5 °C for **2** since the lattice water molecules releases at room temperature. The permittivity as a function of temperature at selected frequencies is displayed in Figure 8e and 8f, respectively. These figures show the existence of discrepancy between the first heating and the next two heating runs, and the distinction between them is due to the lattice water molecules in crystals of **2** removed under N<sub>2</sub> flow. The plots of dielectric permittivity *versus* temperature are almost the same between the second and the third heating runs, indicating that the lattice water molecules were totally removed by N<sub>2</sub> flow during the first heating-cooling run. The dielectric permittivity falls in the ranges of 8.2–10.2 during the first heating run and 7.7–8.7 for the period of the next two heating runs between the temperatures ranges of -150 and -50 °C. The dielectric permittivity increases rapidly when temperature is over -50 °C in three successive heating runs for **2** owing to the orientation of the water molecules in crystal **2** following the change of external electric field. TG and PXRD measurements were further carried out for the pellet of **2** used for dielectric measurement, and the results are almost the same as those of **3**, demonstrating that **2** was transformed into **3** swept by N<sub>2</sub> flow.

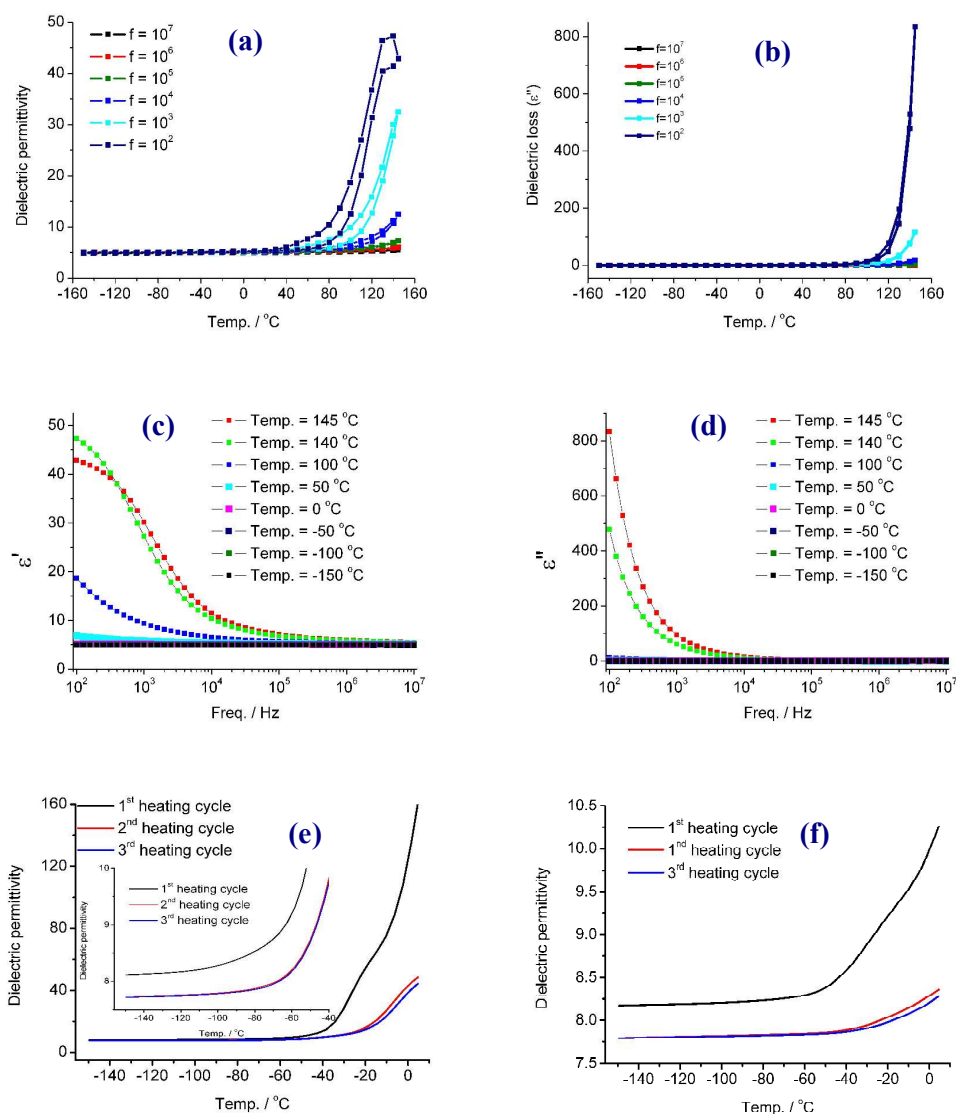


Figure 8 Temperature dependent dielectric permittivity (a)  $\epsilon'$  and (b)  $\epsilon''$  of **1**. Frequency dependent dielectric permittivity (c)  $\epsilon'$  and (d)  $\epsilon''$  of **1**. The dielectric permittivity of **2** at selected ac frequency of (e)  $1.8 \times 10^2$  Hz (f)  $2 \times 10^6$  Hz in three sequentially heating cycle runs (the plot in the 1<sup>st</sup> heating run corresponds to the dielectric behavior of **2**, and the plots in the 2<sup>nd</sup> and 3<sup>rd</sup> correspond to the dielectric behavior of **3**).

## Conclusion

In summary, we successfully achieved two pseudo-polymorphs, Cd(NMIZ)<sub>2</sub>(glutarate) (phase **1**) and [Cd(NMIZ)<sub>2</sub>(H<sub>2</sub>O)(glutarate)]·4H<sub>2</sub>O (phase **2**),

through controlling the crystalline temperature. Crystals of **2** release the lattice water molecules to give the pseudo-polymorph  $\text{Cd}(\text{NMIZ})_2(\text{H}_2\text{O})(\text{glutarate})$  (phase **3**) below 50 °C and further liberate the coordinated water molecules to yield the water-free phase **1**, and phase **1** is able to be transformed into **2** when the crystals of **1** were exposed to excessive moisture. Three pseudo-polymorphs show different dielectric features, and the dielectric permittivity is related to the amount of water in lattice with the order  $\mathbf{2} > \mathbf{3} > \mathbf{1}$ , this is due to that the orientation of polar water molecules in crystal is able to obey the change of external electric field and transfer the polarization.

### **Acknowledgements**

Authors thank the Priority Academic Program Development of Jiangsu Higher Education Institutions and National Nature Science Foundation of China for financial support (grant no. 91122011 and 21271103).

**Notes and references**

1. D. Braga, F. Grepioni, L Maini, M. Polito, *Struct. Bond.* 2009, **132**, 25.
2. J. Bernstein, *Polymorphism in Molecular Crystals*, Clarendon Press: Oxford, 2002.
3. B. Rodríguez-Spong, C. P. Price, A. ayasankar, A. J. Matzger, N. Rodríguez-Hornedo, *Adv. Drug Delivery Rev.* 2004, **56**, 241.
4. R. J. Davey, *Chem. Commun.* 2003, 1463.
5. J. D. Dunitz, J. Bernstein, *Acc. Chem. Res.* 1995, **28**, 193.
6. N. Blagden and R. J. Davey, *Cryst. Growth & Des.* 2003, **3**, 873.
7. C. Avendano, Z. Y. Zhang, A. Ota, H. H. Zhao and K. R. Dunbar, *Angew. Chem. Int. Ed.* 2011, **50**, 6543.
8. N. K. Nath, Aggarwal, H.; Nangia, A. *Cryst. Growth & Des.* 2011, **11**, 967.
9. T. S. Thakur, R. Sathishkumar, A. G. Dikundwar, T. N. Guru Row and G. R. Desiraju, *Cryst. Growth & Des.* 2010, **10**, 4246.
10. M. M. Parmar, O. Khan, L. Seton and J. L. Ford, *Cryst. Growth & Des.* 2007, **7**, 1635.
11. D. Vujovic and L. R. Nassimbeni, *Cryst. Growth & Des.* 2006, **6**, 1595.
12. C. Avendano, Z. Zhang, A. Ota, H. Zhao, K. R. Dunbar, *Angew. Chem.* 2011, **123**, 6673.
13. B.-M. Kukovec, G. A. Venter, C. L. Oliver, *Cryst. Growth Des.* 2012, **12**, 456.
14. Y. Q. Tian, Z. X. Chen, L. H. Weng, H. B. Guo, S. Gao, D. Y. Zhao, *Inorg. Chem.* 2004, **43**, 4631.
15. D. L. Reger, J. R. Gardinier, M. D. Smith, A. M. Shahin, G. J. Long, L. Rebbouh, F. Grandjean, *Inorg. Chem.* 2005, **44**, 1852.
16. H. H.-M. Yeung, M. Kosa, M. Parrinello, P. M. Forster, A. K. Cheetham, *Cryst. Growth & Des.* 2011, **11**, 221.
17. A. Mallick, S. Saha, P. Pachfule, S. Roy, R. Banerjee, *Inorg. Chem.* 2011, **50**, 1392.
18. Y.-s. Kim, H. C. Paskow, R. W. Rousseau *Cryst. Growth & Des.* 2005, **5**, 1623.
19. Z. M. Hao, X. M. Zhang, *Cryst. Growth & Des.* 2007, **7**, 64.

20. F. N. Shi, D. Ananias, T. H. Yang and J. Rocha, *J. Solid State Chem.* 2013, **204**, 321.
21. Á. Monge, F. Gándara, E. Gutiérrez-Puebla and N. Snejko, *CrystEngComm* 2011, **13**, 5031.
22. F. Gándara, V. A. de la Peña-O'Shea, F. Illas, N. Snejko, D. M. Proserpio, E. Gutiérrez-Puebla and M. A. Monge, *Inorg. Chem.* 2009, **48**, 4707.
23. T. K. Prasad, S. Sailaja, M. V. Rajasekharan, *Polyhedron* 2005, **24**, 1487.
24. M. A. Zwijnenburg, R. G. Bell, F. Cora, *J. Solid State Chem.* 2008, **181**, 2480.
25. M. Tabuchi, S. Tsutsui, C. Masquelier, R. Kanno, K. Ado, I. Matsubara, S. Nasu and H. Kageyama, *J. Solid State Chem.* 1998, **140**, 159.
26. J. H. Hong, Y. Oh, Y. Kim, S. K. Kang, J. Choi, Wan S. Kim, J. I. Lee, S.-J. Kim, N. H. Hur, *Cryst. Growth & Des.* 2008, **8**, 1364.
27. Software packages SMART and SAINT, Siemens Analytical X-ray Instrument Inc., Madison, WI, 1996.
28. G. M. Sheldrick, SHELX-97, Program for the refinement of crystal structure, University of Göttingen, Germany, 1997.
29. O. Z. Yeşilel, Y. Kılıç, O. Şahin, O. Büyükgüngör, *Polyhedron* 2014, **67**, 122.
30. Q. Chen, P. C. Guo, S. P. Zhao, J. L. Liu, X. M. Ren, *CrystEngComm* 2013, **15**, 1264.

Table 1: Crystallographic data and refinement parameters for **1** and **2**

Compound	<b>1</b>	<b>2</b>
CCDC no.	1001916	1001917
Temp. (K)	296	296
Wavelength (Å)	0.71073	0.71073
Formula	C <sub>13</sub> H <sub>18</sub> N <sub>4</sub> O <sub>4</sub> Cd	C <sub>13</sub> H <sub>28</sub> N <sub>4</sub> O <sub>9</sub> Cd
Formula weight	406.71	496.79
Space group	<i>P2<sub>1</sub>/c</i>	<i>Pcca</i>
Crystal system	monoclinic	orthogonal
<i>a</i> (Å)	8.9979(9)	16.9674(17)
<i>b</i> (Å)	14.5904(14)	14.2074(14)
<i>c</i> (Å)	13.4092(13)	8.7538(8)
$\alpha$ (°)	90	90
$\beta$ (°)	113.863(6)	90
$\gamma$ (°)	90	90
<i>V</i> (Å <sup>3</sup> ) / <i>Z</i>	1609.9(3) / 4	2110.2(4) / 4
$\rho$ (g·cm <sup>-3</sup> )	1.678	1.564
<i>F</i> (000)	816	1016
Abs.coeff. (mm <sup>-1</sup> )	1.379	1.084
$\theta$ Range for data collection (°)	2.17–25.50	2.796–27.511
Index ranges	-10 ≤ <i>h</i> ≤ 10 -17 ≤ <i>k</i> ≤ 17 -16 ≤ <i>l</i> ≤ 16	-22 ≤ <i>h</i> ≤ 17 -18 ≤ <i>k</i> ≤ 18 -11 ≤ <i>l</i> ≤ 11
<i>R</i> <sub>int</sub>	0.1124	0.0346
Independent /restraints/parameters	reflect. 2984 / 0 / 200	2432 / 0 / 125
Refinement method	The least square refinement on <i>F</i> <sup>2</sup>	
Goodness of fit on <i>F</i> <sup>2</sup>	1.049	1.040
<i>R</i> <sub>1</sub> , <i>wR</i> <sub>2</sub> <sup>a</sup> [ <i>I</i> > 2σ( <i>I</i> )]	0.0466, 0.1319	0.0268, 0.0617
<i>R</i> <sub>1</sub> , <i>wR</i> <sub>2</sub> <sup>a</sup> [all data]	0.0539, 0.1379	0.0428, 0.0679
Residual (e·Å <sup>-3</sup> )	1.457 / -0.990	0.290 / -0.339

$$^a R_1 = \sum ||F_o| - |F_c|| / |F_o|, wR_2 = [\sum w(\sum F_o^2 - F_c^2)^2 / \sum w(F_o^2)^2]^{1/2}$$

Table 2: Typical bond parameters in the coordinate sphere of **1** and **2**

<b>1</b>		<b>2</b>	
Bond distances / Å			
Cd1–N3	2.257(3)	Cd1–O1W	2.230(3)
Cd1–N1	2.267(3)	Cd1–N1	2.288(2)
Cd1–O4#1	2.305(3)	Cd1–N1#1	2.288(2)
Cd1–O2	2.343(3)	Cd1–O1	2.4535(15)
Cd1–O1	2.394(4)	Cd1–O1#1	2.4535(15)
Cd1–O3#1	2.429(3)	Cd1–O2#1	2.4772(17)
		Cd1–O2	2.4772(17)
Bond angles / °			
N3–Cd1–N1	100.51(14)	O1W–Cd1–N1	96.13(5)
N3#1–Cd1–O4	121.53(11)	O1W–Cd1–N1#1	96.13(5)
N1#1–Cd1–O4	87.54(10)	N1–Cd1–N1#1	167.73(10)
N3–Cd1–O2	86.22(10)	O1W–Cd1–O1	136.66(4)
N1–Cd1–O2	96.13(13)	N1–Cd1–O1	84.48(6)
O4#1–Cd1–O2	150.95(11)	N1#1–Cd1–O1	86.60(6)
N3–Cd1–O1	133.36(12)	O1W–Cd1–O1#1	136.66(4)
N1–Cd1–O1	107.10(13)	N1–Cd1–O1#1	86.60(6)
O4#1–Cd1–O1	96.85(12)	N1#1–Cd1–O1 #1	84.48(6)
O2–Cd1–O1	54.77(12)	O1–Cd1–O1#1	86.68(7)
N3–Cd1–O3	89.79(11)	O1W–Cd1–O2#1	84.23(3)
N1#1–Cd1–O3	139.71(11)	N1–Cd1–O2#1	98.04(7)
O4#1–Cd1–O3#1	54.77(11)	N1#1–Cd1–O2 #1	83.30(7)
O2#1–Cd1–O3	123.54(13)	O1–Cd1–O2 #1	138.79(5)
O1#1–Cd1–O3	92.53(13)	O1#1–Cd1–O2 #1	52.69(5)
		O1W–Cd1–O2	84.23(3)
		N1–Cd1–O2	83.20(7)
		N1#1–Cd1–O2	98.04(7)
		O1–Cd1–O2	52.69(5)
		O1#1–Cd1–O2	138.79(5)
		O2#1–Cd1–O2	168.46(7)
Symmetric code: #1 = -1+x, y, z		Symmetric code: #1 = 1-x, y, 2.5-z	